https://doi.org/10.1038/s44407-026-00112-2

Middle East war-driven energy supply disruptions could influence air pollution in India and China

Check for updates

Basudev Swain[1] ✉, Marco Vountas[2] ✉, Luca Lelli[3] ✉, Debashis Tripathy[4], Aishwarya Singh[5], Adrien Deroubaix[6], Ankit Patel[7], Chakradhar Reddy Malasani[7], Ankit Tandon[8] & Sachin S. Gunthe[7]

Rapid economic growth has increased energy demand to ~ 11,000 TWh in India and ~ 50,000 TWh in China, where coal accounts for 57.5% and 54.79% of total energy consumption, respectively. Both countries also depend strongly on imported oil, with ~ 45% of India's and ~ 54% of China's crude-oil imports originating from the Middle East, creating vulnerability to geopolitical energy-supply disruptions. Here, we investigate whether such disruptions could influence regional air pollution by integrating energy data, sector-resolved emissions, GEOS-Chem simulations, and satellite observations. CEDS indicates SO_2 emissions of ~ 9.15 Mt yr^{-1} in India and ~ 10.61 Mt yr^{-1} in China, while GEOS-Chem simulations indicate considerable power-sector contributions to aerosol loading over major energy-producing regions. TROPOMI observations show SO_2 column enhancements of up to ~ 0.6–0.8 DU during the conflict period relative to the corresponding non-conflict reference period. Sulfate constitutes ~ 48% and ~ 42% of aerosol loading over India and China, respectively. However, these SO_2 enhancements cannot be uniquely attributed to increased coal combustion or the Middle East conflict because contemporaneous coal-generation changes were not quantified and atmospheric SO_2 is influenced by multiple emission sources and meteorological processes. The combined evidence therefore identifies a physically plausible pathway through which war-driven geopolitical energy-supply disruptions could influence regional air pollution in India and China.

Rapid economic growth over the past few decades has transformed India and China into two of the largest energy consumers and emitters of air pollutants globally[1–5]. This expansion has been driven by accelerated industrialization, urbanization, and rising living standards, all of which have substantially increased energy demand[6,7]. Despite notable progress in renewable energy deployment, both countries continue to rely heavily on fossil fuels, particularly coal, for electricity generation and industrial activity[8,9]. As a result, India and China consistently experience some of the highest levels of air pollution worldwide, with fine particulate matter ($PM_{2.5}$) posing severe risks to public health, ecosystems, and climate[10–14].

A critical yet often overlooked dimension of air pollution in these regions is its sensitivity to global energy market dynamics. Both India and China are highly dependent on imports of crude oil and natural gas, with a significant proportion sourced from the Middle East[15,16]. This dependence creates a structural vulnerability because geopolitical instability in major energy-exporting regions can disrupt supply chains, alter fuel prices, and potentially influence domestic energy-use decisions [15–17]. In particular, disruptions in oil and gas supply could increase the relative importance of domestically available coal as one potential short-term energy-security response, with possible implications for emissions of sulfur dioxide (SO_2), black carbon, and other pollutants that contribute to secondary aerosol formation and regional air pollution[18].

Recent and ongoing conflicts in the Middle East have raised concerns about the stability of global energy supply systems[19,20]. While the economic and geopolitical implications of such conflicts are widely studied, their potential environmental consequences[20–22], at the same time, indirect impacts on air pollution in distant but energy-dependent regions like India and China remain poorly understood. Existing studies on air pollution over

[1]Department of Physics, University of Oxford, Oxford, UK. [2]Institute of Environmental Physics, University of Bremen, Bremen, Germany. [3]Remote Sensing Technology Institute, German Aerospace Centre (DLR), Wessling, Germany. [4]Department of Chemistry, University of Cambridge, Cambridge, UK. [5]Max Planck Institute for Chemistry, Mainz, Germany. [6]Max-Planck-Institut für Meteorologie, Hamburg, Germany. [7]CACS, Indian Institute of Technology Madras, Chennai, India. [8]Department of Environmental Sciences, Central University of Jammu, Samba, India. ✉e-mail: basudev.swain@physics.ox.ac.uk; vountas@iup.physik.uni-bremen.de; luca.lelli@dlr.de

these countries have primarily focused on local emission sources, policy interventions, and meteorological influences[10–14,18,23–28], with limited attention given to how external geopolitical shocks can propagate through energy systems and influence further air pollution.

In this context, the present study investigates whether energy disruptions coinciding with the Middle East conflict are associated with, and could plausibly contribute to, changes in air pollution in India and China. We examine long-term changes in economic growth and energy consumption, quantify the role of fossil fuel based energy production in driving emissions, and compare atmospheric sulfur dioxide observed by satellite in March 2025, one year before the conflict, with March 2026, during the ongoing conflict. By linking energy system dynamics with air pollution, this study provides a comprehensive framework for understanding how external geopolitical events can influence regional air pollution.

The importance of this work lies in its ability to bridge the gap between energy security, geopolitics, and environmental sustainability in terms of regional air pollution. First, it highlights a previously underexplored pathway through which distant geopolitical conflicts can indirectly influence air pollution in major emerging economies. Second, it underscores the risks associated with continued dependence on fossil fuels, particularly coal, as a fallback option during energy supply disruptions. Third, it provides observational and process-based evidence that can inform policymakers about the environmental consequences of energy choices made under geopolitical crisis conditions.

Understanding these interconnections is crucial for developing resilient energy systems capable of withstanding external shocks without compromising air pollution and public health. As India and China continue to experience rapid economic growth, their energy demand is increasing correspondingly, further intensifying pressure on existing energy systems. Reducing vulnerability to such disruptions will require diversification of energy sources, accelerated deployment of renewable energy, and strengthened emission control measures. More broadly, this study highlights the importance of integrating geopolitical risks into air pollution and climate policy frameworks, particularly within an increasingly interconnected global energy system.

Results

Rapid economic boom is driving energy consumption in India and China

Sustained economic growth in India and China over the past three decades has been tightly coupled with a rapid expansion in energy demand, particularly electricity consumption (Fig. 1a, b). In India, GDP per capita increased from ~ US$300 in the 1960s to ~ US$2300–2400 by 2023, while electricity demand rose from negligible levels to ~ 2000–2200 TWh (Fig. 1a). China exhibits a much steeper trajectory, with GDP per capita rising from < US$500 to > US$12,000, accompanied by a surge in electricity demand to ~ 10,000 TWh (Fig. 1b). The strong co-evolution of GDP and electricity demand, especially after the late 1990s, demonstrates that economic growth in both countries remains highly energy-intensive, with strong coupling between development and energy use (Fig. 1a, b).

This growth has been supported by a massive expansion in total energy consumption (Fig. 1c, d). India's energy use increased from < 1000 TWh in 1965 to > 11,000 TWh in 2024, whereas China's rose from ~ 1000 TWh to nearly 50,000 TWh over the same period, indicating a fivefold larger energy system in China (Fig. 1c, d). The composition of this energy use is dominated by fossil fuels, particularly coal, which contributes 57.5% of total energy consumption in India and 54.79% in China. Oil constitutes the second-largest share (27.56% in India; 19.78% in China), while natural gas contributes relatively modest fractions (5.8% and 8.8%, respectively). Despite recent growth in renewables and nuclear energy, their individual contributions remain comparatively small, indicating that fossil fuels continue to underpin the energy systems of both countries (Fig. 1c,d).

Despite the rapid expansion of renewable energy, coal remains the largest component of the present energy mix, accounting for approximately 57.5% of total energy consumption in India and 54.79% in China (Fig. 1c,d). Its continued importance is further reflected in the extensive existing coal-fired power-generation infrastructure across both countries (Fig. 1e,f). In India, coal-fired power plants are concentrated across the Indo-Gangetic Plain, eastern coal-bearing regions (Jharkhand and Odisha), and central India (Chhattisgarh and Madhya Pradesh), with plant capacities ranging from ~ 50 MW to > 1000 MW (Fig. 1e). In China, thermal power plants are more densely distributed across eastern and northern industrial regions, including the North China Plain and coastal economic zones (Fig. 1f), reflecting the larger scale of its industrial and energy system. Consequently, although renewable energy is becoming increasingly important for long-term energy diversification, the scale and availability of the existing coal-fired power fleet continue to make coal a major component of the current energy systems of India and China. This extensive infrastructure also provides the capacity for increased utilization of existing coal-based generation during periods of short-term energy-supply uncertainty, while potentially reinforcing dependence on high-emission infrastructure.

In parallel with domestic production, both countries exhibit significant dependence on imported fossil fuels, particularly oil and natural gas (Fig. 1g,h). India imports approximately 80–90% of its crude oil, ~ 50% of its natural gas, and ~ 20–30% of its coal demand (Fig. 1g). China, while largely self-sufficient in coal, still relies heavily on imports for oil and natural gas, with coal imports playing a comparatively smaller role (Fig. 1h). The structure of these imports reveals strong geopolitical linkages. The Middle East supplies ~ 45% of India's and ~ 54% of China's crude-oil imports (Fig. 1i), with major contributors including Iraq (19%) and Saudi Arabia (16%) for India, and Saudi Arabia (14%), Iraq (10%), Iran (11%), Oman (7%), and the United Arab Emirates (6%) for China. Natural gas imports are more diversified, with China sourcing from Australia (40.4%), the United States (17.0%), Qatar (15.1%), and Russia (14.0%), whereas India depends heavily on Qatar (50%), followed by the United States (14.0%) and the United Arab Emirates (12%). Coal imports in both countries are dominated by Indonesia (42% for India and 46% for China), with additional contributions from Australia, Russia, and South Africa (Fig. 1i). This substantial dependence on Middle Eastern crude oil creates an energy-security exposure through which geopolitical instability, supply disruptions, or associated changes in international energy prices could influence domestic energy availability and fuel-use decisions. However, the magnitude of such impacts depends on the severity and duration of the disruption, access to alternative suppliers, availability and use of strategic reserves, domestic production, market adaptation, and government policy responses. In this context, energy vulnerability refers to the exposure of a national energy system to external supply disruptions arising from its dependence on imported fuels. The combination of substantial oil and natural-gas import dependence with large domestic coal-based energy systems creates a structural vulnerability in India and China, whereby external supply shocks could influence domestic fuel-use decisions.

These results demonstrate that rapid economic expansion in India and China has driven a sustained increase in energy consumption, dominated by coal and supported by extensive thermal power infrastructure and global fuel supply chains from Middle East. The strong coupling between economic growth, fossil fuel dependence, and import reliance highlights a structural vulnerability of external disruptions in energy supply, particularly from geopolitically sensitive regions of Middle East can directly influence domestic energy use patterns, with important implications for emissions and air pollution.

Energy production from fossil fuels is creating air pollution

The expansion of fossil fuel-based energy production in India and China has been accompanied by substantial emissions of sulfur dioxide (SO_2), an important precursor of sulfate aerosol and secondary particulate matter (Fig. 2a, b). Long-term sectoral time series from the Community Emissions Data System (CEDS) show that the energy and industrial sectors constitute major sources of SO_2 emissions in both countries (Fig. 2a, b). In India, SO_2 emissions increased substantially over the historical period, reaching ~ 9.15 million tonnes yr^{-1} in 2023, with the energy sector representing the largest

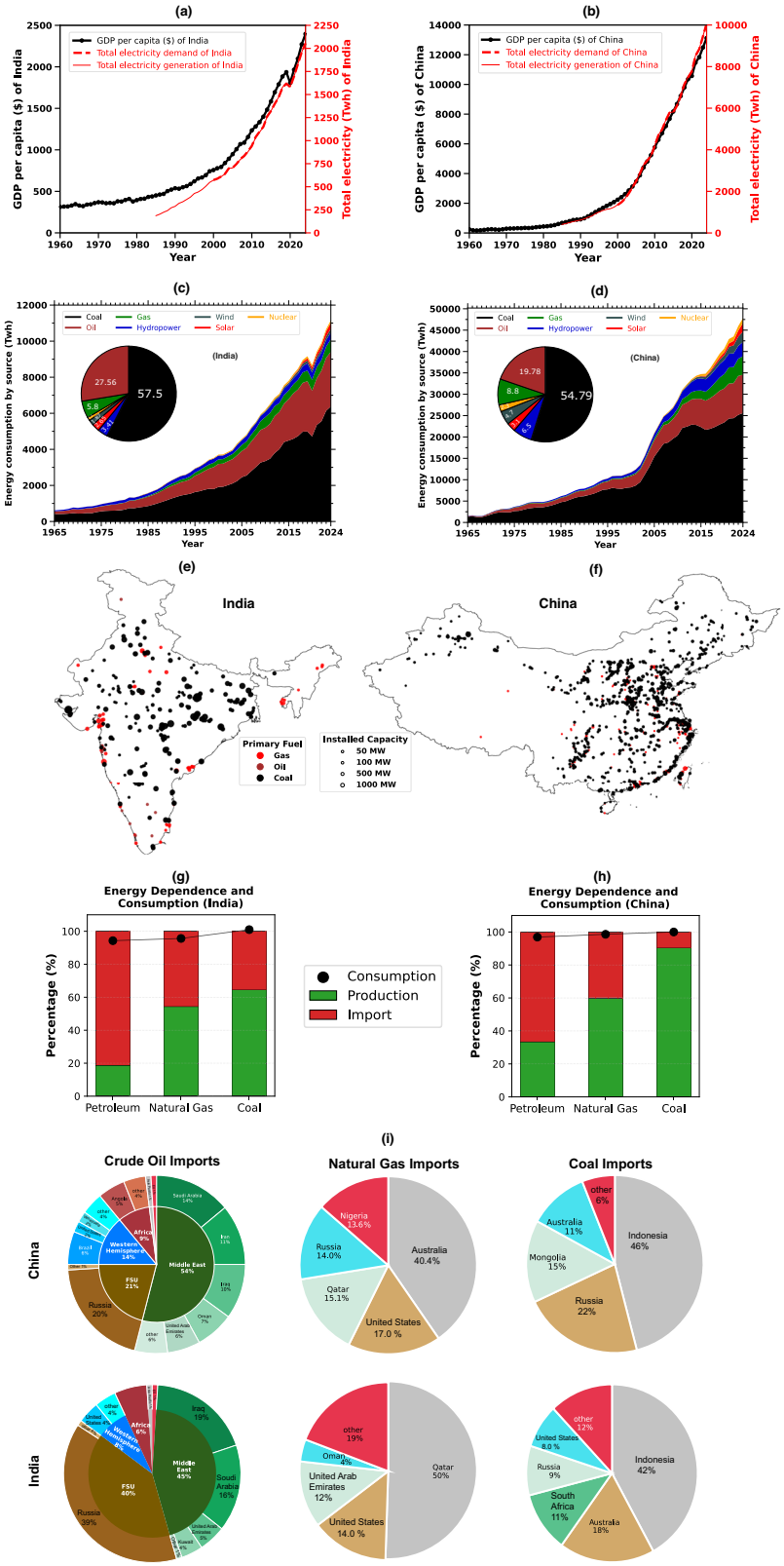

Fig. 1 | Energy consumption, infrastructure, and import dependence of India and China. a, **b** Long-term time-series (1960-2023) in gross domestic product (GDP) per capita and total electricity demand and generation for India (**a**) and China (**b**), highlighting rapid economic growth coupled with rising energy demand. **c**, **d** Evolution of energy consumption by source (coal, oil, gas, hydropower, nuclear, wind, and solar) for India (**c**) and China (d), with inset pie charts showing the relative contributions of major energy sources in recent year of 2023, dominated by coal in both countries. **e**, **f** Spatial distribution of thermal power plants across India (**e**) and China (**f**), categorized by primary fuel type and installed capacity, illustrating the widespread reliance on coal-based infrastructure. Energy dependence profiles for India (**g**) and China (**h**), showing the proportions of domestic production, consumption, and imports for petroleum, natural gas, and coal. **i** Composition of fossil fuel imports, including crude oil, natural gas, and coal, for both countries, highlighting strong dependence on external suppliers–particularly Middle Eastern sources for crude oil and diversified global sources for gas and coal. Together, these panels demonstrate the structural dependence of India and China on fossil fuels and imported energy, underscoring their vulnerability to external geopolitical shocks.

contribution in recent decades (Fig. 2a). China experienced a more rapid increase during its period of industrialization, with total SO_2 emissions peaking at approximately ~20 million tonnes yr^{-1} in the early 2010s before declining to ~10.61 million tonnes yr^{-1} in 2023. The recent decline in China is consistent with the implementation of stringent emission-control measures, although the remaining SO_2 burden continues to be associated substantially with fossil-fuel-based energy and industrial activities (Fig. 2a,b).

The spatial distributions of CEDS SO_2 emissions further illustrate the relationship between energy production and regional emission hotspots

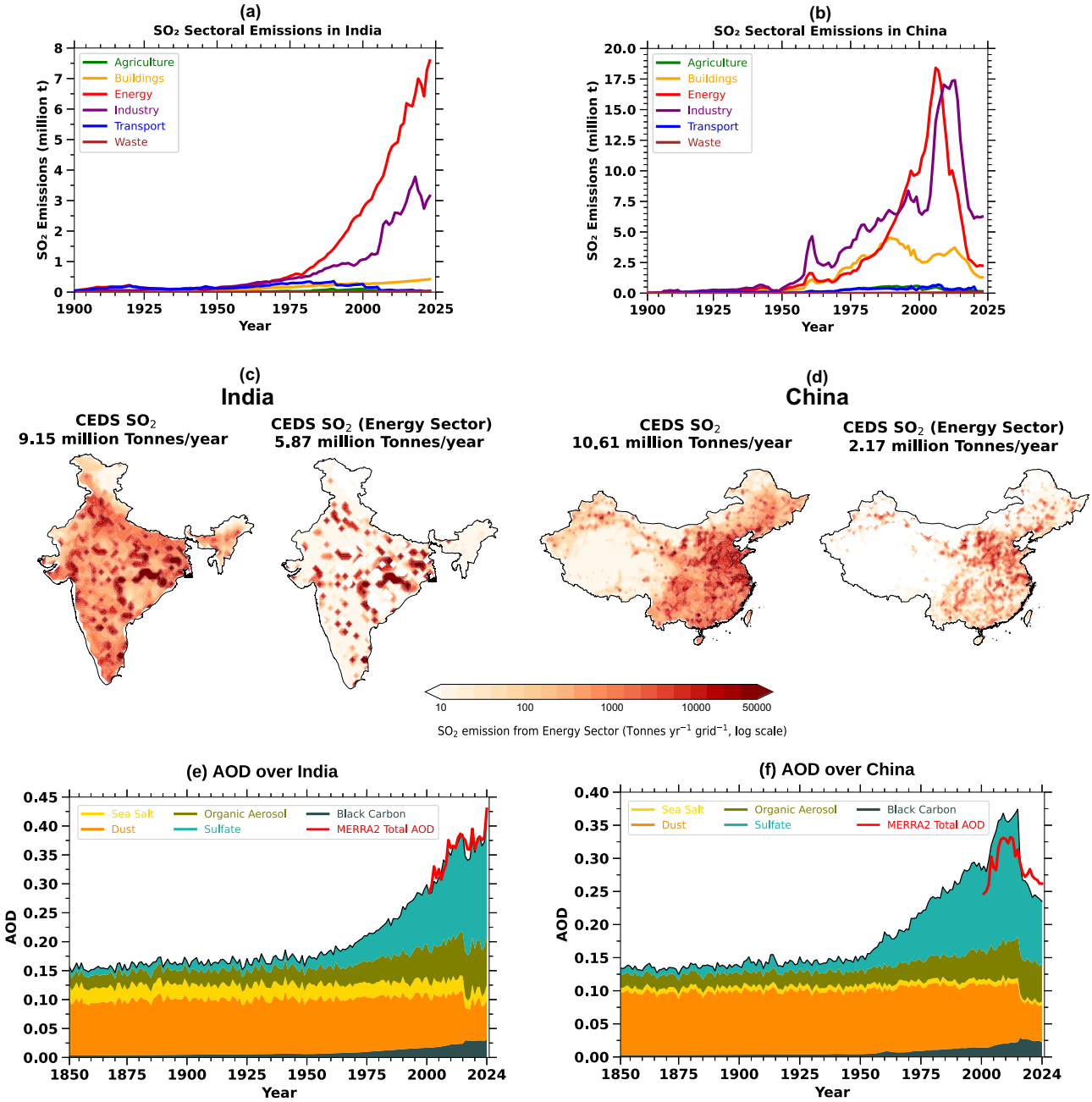

Fig. 2 | Sectoral SO_2 emissions, spatial distribution, and long-term aerosol evolution in India and China. Historical sectoral sulfur dioxide (SO_2) emissions (1900–2023) for India (**a**) and China (**b**), showing dominant contributions from the energy and industrial sectors, with China exhibiting a peak (~ 20 million tonnes yr^{-1}) in the early 2010s followed by a decline, while India shows a steady increase (~ 9.15 million tonnes yr^{-1} in 2023). Spatial distribution of total SO_2 emissions and energy sector contributions in 2023, highlighting major emission hotspots over coal-fired power plant regions in India (**c**) and China (**d**), with the energy sector contributing ~ 5.87 and ~ 2.17 million tonnes yr^{-1}, respectively. Long-term evolution of aerosol optical depth (AOD) and its components over India (**e**) and China (**f**), constructed from historical model output and extended beyond the historical period using the CMIP6 SSP2-4.5 scenario. The post-historical portion therefore represents scenario-based model output rather than observed AOD.

(Fig. 2c,d). In India, total emissions (~ 9.15 million tonnes yr^{-1}) are distributed across the country, but pronounced hotspots occur over the Indo-Gangetic Plain, the eastern coal belt (Jharkhand–Odisha), and central India, including Chhattisgarh, where coal-based thermal power generation and industrial activities are concentrated (Fig. 2c). Similarly, China's total SO_2 emissions (~ 10.61 million tonnes yr^{-1}) are spatially widespread, with enhanced emission densities over major industrial and energy-producing regions, including the North China Plain, the Yangtze River Delta, and the Sichuan Basin (Fig. 2d).

The importance of energy production becomes clearer when the energy-sector component of CEDS SO_2 emissions is considered separately (Fig. 2c,d). CEDS sectoral emissions indicate that energy production and industrial activity represent major anthropogenic sources of SO_2 in both India and China, while energy-sector emissions are more spatially localized and show substantial correspondence with regions containing dense coal-fired power infrastructure. In 2023, the energy sector contributed approximately ~ 5.87 million tonnes yr^{-1} of SO_2 in India and ~ 2.17 million tonnes yr^{-1} in China. These spatial patterns indicate that fossil-fuel-based

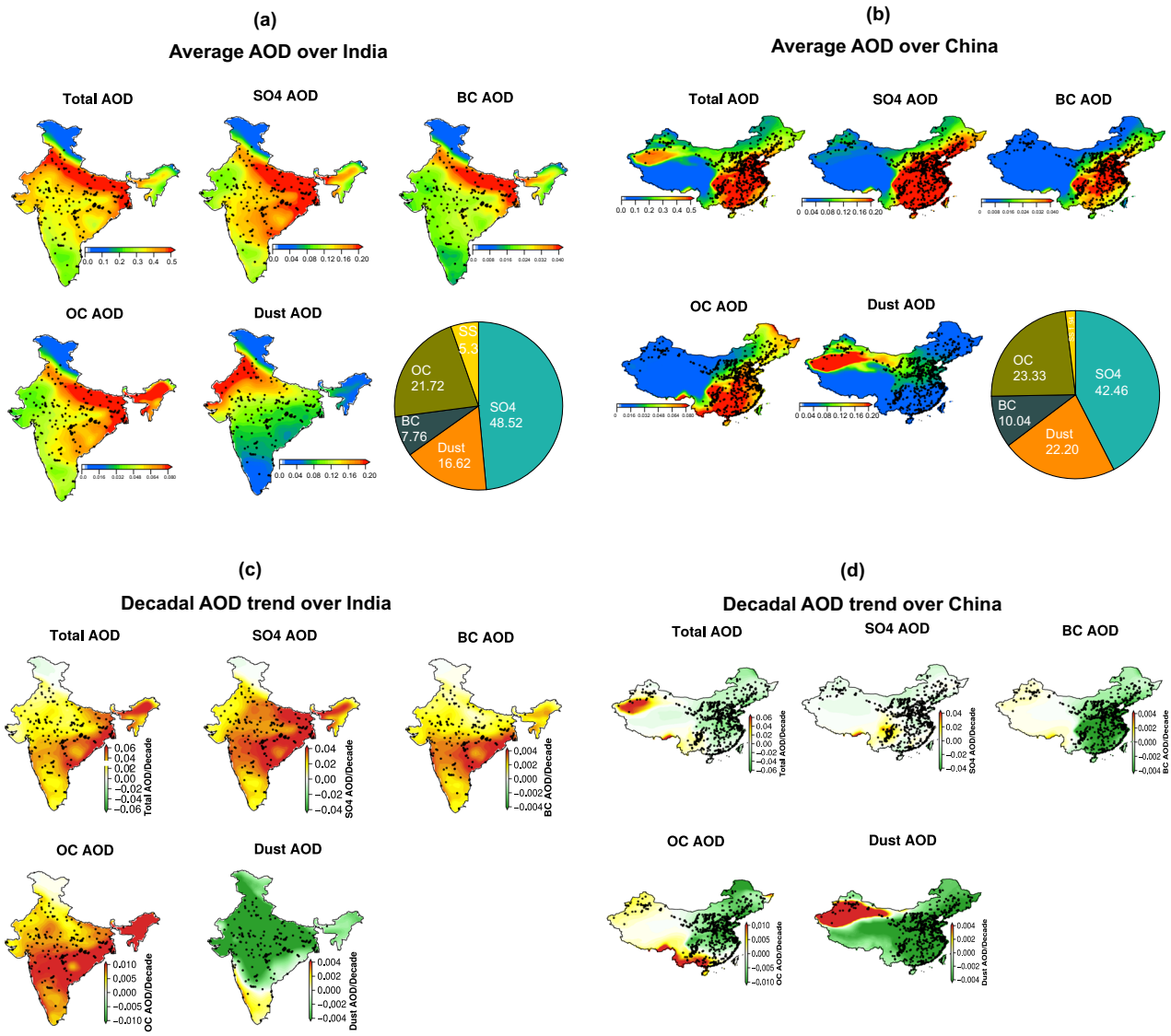

Fig. 3 | Spatial distribution and trends of aerosol optical depth and its components over India and China from MERRA-2. Multi-year mean (2000–2024) total AOD and its model-derived aerosol components (sulfate, black carbon, organic carbon, and dust) over India (**a**) and China (**b**). Pie charts show the relative contributions of the aerosol components, with sulfate representing the largest fraction in both countries. Decadal trends in total and speciated AOD during 2000–2024 over India (**c**) and China (**d**). India exhibits predominantly positive trends in total and sulfate AOD across several regions, whereas China shows spatially heterogeneous, generally decreasing or near-neutral trends across several eastern regions. Black dots indicate the locations of coal-fired thermal power plants.

power generation represents an important source of regional sulfur emissions, particularly within major coal-dependent energy corridors. However, industrial activities and other anthropogenic sectors also contribute to the total SO_2 burden; therefore, variations in atmospheric SO_2 should not be attributed exclusively to power-sector emissions.

The atmospheric aerosol record is consistent with the substantial anthropogenic emission burden in both countries. The long-term evolution of aerosol optical depth (AOD) and its components (Fig. 2e,f) shows an increase in total AOD from approximately ~0.1 in the mid-20th century to ~ 0.35–0.40 in recent decades. China, however, exhibits a noticeable reduction in AOD during recent years, consistent with the implementation of stringent clean-air policies and emission-control technologies. The compositional analysis indicates that sulfate represents the largest fraction of the aerosol burden, contributing 48.52% over India and 42.46% over China. Organic carbon contributes 21.72% and 23.33%, dust contributes 16.62% and 22.20%, and black carbon contributes 7.76% and 10.04% over India and China, respectively, while sea salt contributes comparatively smaller fractions (5.3% and 1.94%). The resulting aerosol burden therefore reflects contributions from both anthropogenic and natural sources. The predominance of sulfate is consistent with the importance of anthropogenic SO_2 emissions, including those associated with fossil-fuel combustion, while organic carbon and black carbon represent additional anthropogenic and combustion-related contributions. Dust and sea salt further demonstrate the contribution of natural aerosol sources to total AOD. Thus, regional AOD should be interpreted as the combined influence of emissions, atmospheric processing, and natural aerosol sources rather than as a measure of fossil-fuel pollution alone[14,29].

The spatial distribution of AOD from MERRA-2 further characterizes the regional aerosol burden associated with major energy and industrial regions (Fig. 3a,b). The 2000–2024 mean distributions show persistently elevated aerosol loading over regions containing dense coal-fired power infrastructure in both countries. In India, average total AOD reaches approximately ~ 0.35–0.40 across the Indo-Gangetic Plain, eastern India, and parts of central India, with sulfate contributing approximately 48.5% of the total AOD. Organic carbon (~ 21.7%) and dust (~ 16.6%) provide additional substantial contributions, while black carbon accounts for ~7.8%

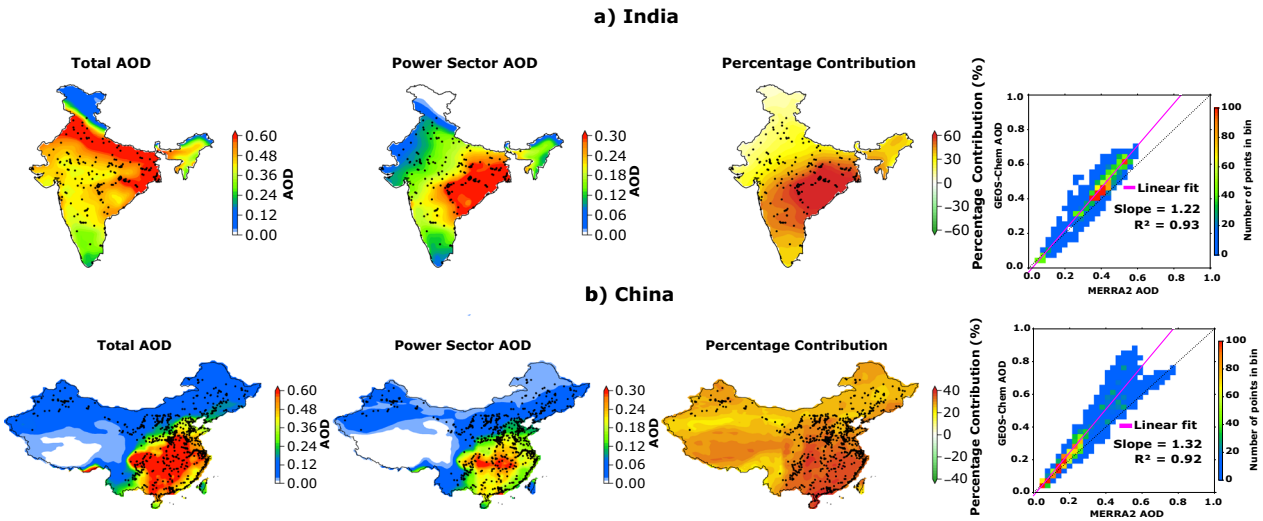

Fig. 4 | Power-sector contribution to aerosol optical depth over India and China simulated using GEOS-Chem. Spatial distributions of total aerosol optical depth (AOD), power-sector-attributable AOD, and the percentage contribution of the power sector to total AOD over India (**a**) and China (**b**), simulated using the GEOS-Chem chemical transport model. Black dots indicate the locations of coal-fired thermal power plants. The rightmost panels evaluate the GEOS-Chem simulated total AOD against MERRA-2 AOD, showing strong spatial agreement for India (R^2 = 0.93; slope = 1.22) and China (R^2 = 0.92; slope = 1.32). The simulations demonstrate substantial contributions of power-sector emissions to aerosol loading, particularly over regions with dense coal-fired power generation and industrial activity.

(Fig. 3a). In China, elevated mean AOD (~ 0.4–0.5) occurs predominantly across eastern and northern China, where thermal power plants and industrial activities are concentrated (Fig. 3b). Sulfate again represents the largest component (~ 42.5%), followed by organic carbon (~ 23.3%) and dust (~ 22.2%). Although spatial co-location alone cannot establish source attribution, the correspondence between regions of enhanced aerosol loading and major fossil-fuel-based energy and industrial regions motivates a quantitative assessment of the power-sector contribution.

The trend analysis of MERRA-2 AOD and its components during 2000–2024 provides further insight into the temporal evolution of aerosol loading (Fig. 3c,d). Over India, total AOD exhibits positive trends of ~ 0.02–0.06 per decade across substantial parts of the country, with pronounced increases over several coal-dominated energy and industrial regions (Fig. 3c). Sulfate AOD shows positive trends of ~ 0.01–0.04 per decade, while organic carbon exhibits increases of up to ~ 0.01 per decade and black carbon shows more moderate increases (~ 0.001–0.004 per decade). Dust exhibits comparatively weak or locally negative trends (up to ~ − 0.004 per decade). The statistical significance analysis (Fig. S1) indicates that positive trends in total and sulfate AOD are statistically significant across several regions, demonstrating a sustained increase in anthropogenic aerosol loading over parts of India.

China exhibits a contrasting and spatially heterogeneous evolution (Fig. 3d). Total AOD shows decreasing or near-neutral trends of ~− 0.02 to 0.00 per decade across several regions, particularly over eastern China, consistent with the effects of emission-control policies [14,29]. Sulfate trends are weakly negative to near-neutral (~ − 0.02 to 0.01 per decade), while black carbon exhibits localized declines of approximately ~ − 0.001 to − 0.004 per decade. Organic carbon displays spatially mixed trends, with increases of approximately ~ 0.005–0.01 per decade in some regions, whereas dust trends vary spatially (~ ± 0.004 per decade). The statistical significance analysis (Fig. S2) further indicates that reductions in total and sulfate AOD are spatially heterogeneous, emphasizing substantial regional differences in the evolution of aerosol loading.

Overall, the MERRA-2 trends during 2000–2024 reveal contrasting aerosol trajectories over India and China (Fig. 3c,d). India exhibits predominantly positive trends in total and sulfate AOD across several major energy and industrial regions, indicating a sustained increase in aerosol loading over parts of the country. In contrast, China shows decreasing or near-neutral trends across several eastern regions, consistent with the effects of emission-control policies, although the magnitude and statistical significance of these changes remain spatially heterogeneous. Furthermore, these contrasting trajectories indicate that the atmospheric consequences of fossil-fuel use depend not only on the magnitude of energy consumption but also on the implementation and effectiveness of emission-control policies and technologies.

Taken together, these results indicate that the continued dependence on fossil fuels has important implications for regional air quality, as energy and industrial activities represent major sources of SO_2 emissions (Fig. 2), while sulfate constitutes approximately 48.5% and 42.5% of the aerosol burden over India and China, respectively (Fig. 3). Many regions characterized by enhanced SO_2 emissions and aerosol loading spatially correspond with the major coal-fired power-generation regions identified in Fig. 1e,f, including the Indo-Gangetic Plain, eastern and central India, and major industrial regions of eastern and northern China. SO_2 is an important precursor of secondary sulfate aerosol, with atmospheric oxidation of SO_2 contributing to sulfate formation and subsequent particulate aerosol loading. The predominance of sulfate is therefore consistent with the importance of anthropogenic sulfur emissions, including those associated with fossil-fuel combustion. However, the resulting sulfate aerosol burden does not depend on SO_2 emissions alone, as atmospheric chemistry, transport, meteorological conditions, and removal processes also regulate sulfate formation and accumulation[14,30]. Furthermore, the CEDS and MERRA-2 analyses alone do not provide quantitative attribution of the observed aerosol loading to individual emission sectors. We therefore use GEOS-Chem simulations to quantify the contribution of power-sector emissions to regional AOD (Fig. 4), providing a process-based assessment of the role of fossil-fuel-based power generation in regional aerosol loading.

To quantify more explicitly the contribution of power-sector emissions to regional aerosol loading, we performed GEOS-Chem[31] simulations for 2023, from which total AOD and power-sector-attributable AOD were quantified (Fig. 4). The year 2023 was selected because the sector-resolved CEDS emission inventory[32] used to constrain the GEOS-Chem simulations is currently available only through 2023. The simulations reveal a substantial spatial correspondence between enhanced power-sector AOD and regions containing dense coal-fired power-generation infrastructure in both countries (Fig. 4a,b). Over India, enhanced power-sector AOD is particularly evident across eastern and central India and parts of the Indo-Gangetic Plain, resulting in substantial percentage contributions of the power sector

to total simulated AOD in these regions. Over China, the power-sector contribution is concentrated predominantly across eastern and northern China, where thermal power generation and industrial activity are particularly dense. The percentage-contribution maps therefore provide a model-based quantitative estimate of the importance of power-generation emissions to regional aerosol loading and complement the spatial correspondence identified independently from CEDS emissions and MERRA-2 AOD.

The representation of regional aerosol loading by GEOS-Chem was further evaluated against MERRA-2 AOD (Fig. 4a,b, right panels). The comparison demonstrates strong spatial correspondence between GEOS-Chem and MERRA-2, with R^2 = 0.93 and a regression slope of 1.22 over India and R^2 = 0.92 with a slope of 1.32 over China. Although the slopes greater than unity indicate that GEOS-Chem tends to simulate higher AOD than MERRA-2 across the comparison range, the high coefficients of determination demonstrate that the model reproduces the dominant spatial variability in regional aerosol loading. This positive model bias introduces uncertainty into the absolute magnitude of the simulated power-sector contribution. Moreover, because the attribution is derived from a power-sector zero-out experiment, the resulting percentages represent the modeled response to removing that sector and may include nonlinear responses in secondary aerosol formation. The percentage contributions in Fig. 4 should therefore be interpreted as approximate model-derived attribution estimates rather than exact observational source fractions. Together, the CEDS sectoral emission distributions, MERRA-2 aerosol fields, and GEOS-Chem source-attribution simulations provide complementary evidence that power-sector emissions make an important contribution to aerosol loading over major fossil-fuel-based energy-producing regions of India and China (Figs. 2–4).

Importantly, we restrict the quantitative GEOS-Chem power-sector attribution to 2023 rather than extrapolating these simulations to the subsequent Middle East conflict period. The most recent CEDS release used in this study extends the sector-resolved emission estimates through 2023, and therefore the magnitude and spatial distribution of post-2023 changes in power-sector emissions cannot be constrained consistently within the same emission-inventory framework[32]. Extending the 2023 simulation to the conflict period using an assumed scaling factor would require prescribing a priori the magnitude and spatial distribution of changes in coal-fired generation and associated emissions. Such an approach would provide limited independent information because the resulting modeled aerosol response would depend directly on the imposed emission perturbation. Furthermore, atmospheric aerosol loading cannot necessarily be inferred from a simple proportional scaling of power-sector emissions. Secondary aerosol concentrations are controlled by coupled processes involving precursor emissions, atmospheric chemistry, thermodynamic partitioning, transport, and wet and dry removal, and their response can additionally depend on meteorological conditions [30,31]. Consequently, sensitivity simulations based on prescribed emission scaling are useful for testing the atmospheric response to a specified perturbation, but they do not independently establish that such an emission perturbation occurred[30]. In the absence of an observationally constrained post-2023 sectoral emission inventory, applying an arbitrary scaling factor to the 2023 CEDS power-sector emissions could therefore introduce additional assumptions into the attribution rather than provide a robust quantitative estimate of conflict-period aerosol changes.

We consequently use the 2023 GEOS-Chem simulations to establish the contribution of power-sector emissions to the underlying aerosol burden, but do not prescribe a model-based conflict-period emission perturbation. Instead, our assessment of atmospheric changes during the ongoing Middle East conflict relies primarily on TROPOMI observations of SO_2, which provide a satellite observation of the spatial and temporal variability of atmospheric sulfur during the period of interest. In the following section, these observations are considered together with the energy-import vulnerability of India and China, the spatial distribution of coal-fired power infrastructure, and meteorological variability to assess whether the recent atmospheric SO_2 changes are consistent with the proposed pathway linking Middle East energy-supply disruptions, increased reliance on coal-based energy, and deterioration of regional air quality (Figs. 5 and 6).

Potential air-pollution implications of energy-supply disruptions in India and China

Ongoing geopolitical instability in the Middle East has the potential to disrupt global energy markets, particularly the supply and price of crude oil and natural gas on which India and China remain strongly dependent (Fig. 1). Such disruptions create a potential pathway through which energy-security responses could alter domestic fuel use. Because coal represents a major domestically available component of the energy systems of both countries, reduced availability or increased cost of imported oil and gas could increase the incentive to utilize existing coal-fired generation capacity. The proposed mechanism is illustrated schematically in Fig. 5a: disruption of Middle Eastern oil and gas supplies may increase reliance on coal-based energy production, potentially enhancing SO_2 emissions and, through atmospheric oxidation, sulfate aerosol and secondary particulate matter ($PM_{2.5}$). Importantly, this represents a hypothesized energy–emission pathway rather than, by itself, evidence of causality.

The plausibility of this pathway is supported by the energy structure described in Fig. 1. Coal accounts for 57.5% of total energy consumption in India and 54.79% in China (Fig. 1c,d), and both countries possess extensive existing coal-fired power-generation infrastructure (Fig. 1e,f). In contrast, crude-oil supply remains strongly dependent on external sources, with Middle Eastern countries contributing approximately 45% of India's and 54% of China's crude-oil imports (Fig. 1i). Disruptions to imported oil and gas could therefore increase the relative importance of domestically available coal as one component of a short-term energy-security response. Because substantial coal-fired generating capacity is already operational, existing plants could potentially be utilized more intensively where technical capacity, coal availability, electricity demand, grid requirements, and environmental regulations permit[33–35]. Importantly, this mechanism does not imply a direct or proportional substitution of oil and gas by coal, because these fuels serve different end uses and the actual response may be moderated by alternative suppliers, strategic reserves, domestic production, renewable-energy availability, market adaptation, and government policy. We therefore consider increased coal utilization as one plausible response pathway rather than an inevitable consequence of Middle Eastern energy-supply disruption.

We next examine whether atmospheric SO_2 changed during the period coinciding with the ongoing Middle East conflict using TROPOMI satellite observations (Fig. 5b,c). Rather than prescribing an assumed conflict-related emission perturbation in GEOS-Chem, as discussed in the preceding section, this analysis directly compares the observed atmospheric SO_2 distribution between March 2025, used here as the pre-conflict reference period, and March 2026, representing the conflict period. Over India, TROPOMI shows widespread positive differences in SO_2 column density between March 2025 and March 2026 (Fig. 5b). Pronounced enhancements occur over parts of the Indo-Gangetic Plain, the eastern coal-producing regions of Jharkhand and Odisha, and central India, including Chhattisgarh and surrounding regions. Many of these locations coincide spatially with dense clusters of coal-fired thermal power plants (Fig. 5b). Localized differences reach ~0.6–0.8 DU, indicating a substantial enhancement in atmospheric SO_2 column abundance during March 2026 relative to March 2025.

A comparable enhancement is apparent over China (Fig. 5c). Positive March 2026 minus March 2025 SO_2 differences occur across substantial parts of eastern and northern China, including regions associated with the North China Plain and other major power-generation and industrial corridors. Several of these enhancements are spatially co-located with dense coal-fired power infrastructure, with localized differences approaching approximately 0.8 DU (Fig. 5c). The spatial correspondence between enhanced SO_2 columns and major coal-dependent energy regions in both countries is therefore consistent with the proposed mechanism in Fig. 5a. However, spatial correspondence alone does not establish that increased

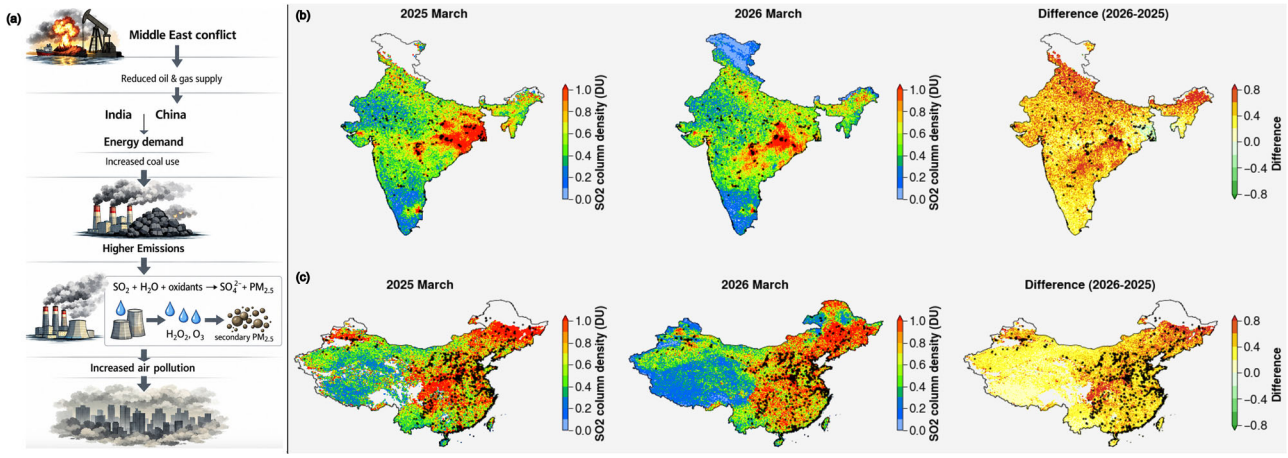

Fig. 5 | Potential impact of Middle East conflict–related energy disruption on air pollution in India and China. a Conceptual framework illustrating the proposed pathway linking Middle East energy-supply disruption to regional air pollution, whereby reduced availability or increased cost of imported oil and gas could increase the relative importance of coal-based energy production, potentially enhancing SO_2 emissions and subsequent sulfate aerosol and secondary particulate matter ($PM_{2.5}$) formation. **b** TROPOMI observations showing the spatial distribution of mean SO_2 column density over India for 1–20 March 2025 (pre-conflict/reference period) and the corresponding 1–20 March 2026 period (conflict period), together with the 2026 minus 2025 difference calculated using the same 20-day sampling window. **c** Same as in (**b**), but for China. Positive differences are observed over several regions containing substantial coal-fired power infrastructure; however, the satellite observations represent atmospheric SO_2 column abundance and do not independently establish the emission source or cause of the observed enhancement. Black dots indicate the locations of coal-fired thermal power plants.

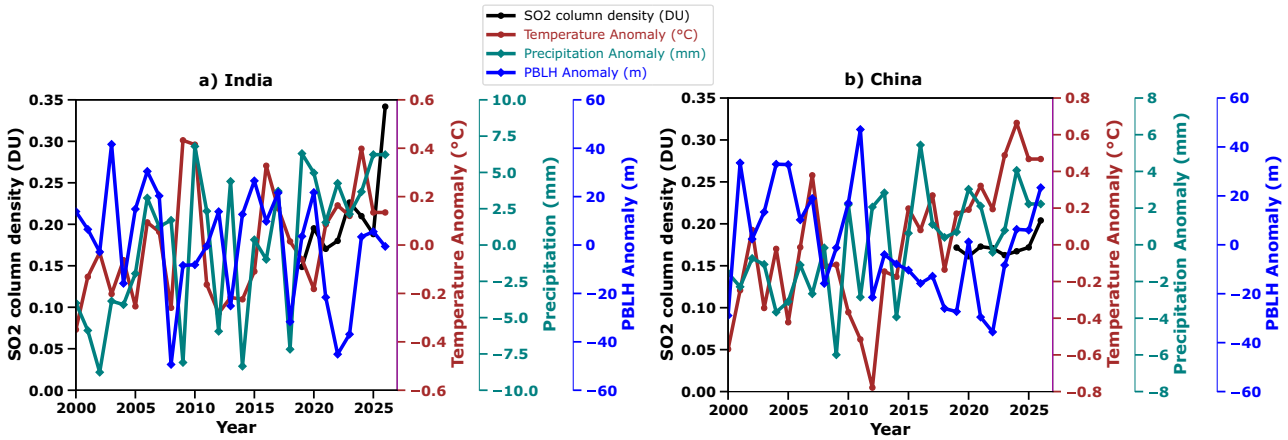

Fig. 6 | TROPOMI SO_2 variability and meteorological conditions over India and China. Temporal variability in TROPOMI-observed SO_2 column density together with temperature, precipitation, and planetary boundary-layer height (PBLH) anomalies over India (**a**) and China (**b**). TROPOMI SO_2 observations are shown for 2019–2026, with each annual value calculated using quality-filtered observations over the same 1–20 March period to ensure a consistent calendar-day sampling window across years. Near-surface temperature and precipitation are obtained from CRU TS, while PBLH is obtained from ERA5. The meteorological records are shown for 2000–2026 to provide a longer-term context for interannual variability. Temperature, precipitation, and PBLH anomalies are expressed relative to their respective mean conditions over the 2000–2026 analysis period. The comparison provides meteorological context for interpreting the recent SO_2 variability but is not intended to provide a complete meteorological normalization or causal attribution of the observed SO_2 changes.

coal combustion caused the observed enhancement, because TROPOMI measures atmospheric SO_2 columns rather than sector-specific emission fluxes.

To place the March 2025–March 2026 SO_2 differences in a broader temporal and meteorological context, we examine the available TROPOMI SO_2 record together with temperature, precipitation, and planetary boundary-layer height (PBLH) anomalies over India and China (Fig. 6). Figure 5 provides the spatial comparison between March 2025 and March 2026, whereas Fig. 6 provides the complementary multi-year temporal context for evaluating the recent SO_2 behavior. The addition of PBLH provides information on variations in atmospheric mixing depth that may influence pollutant accumulation and dilution. Over India, the SO_2 time series shows an increase toward 2026 relative to the immediately preceding period (Fig. 6a). The corresponding meteorological records exhibit substantial interannual variability; however, the recent SO_2 behavior does not show a simple correspondence with temperature, precipitation, or PBLH alone. These comparisons do not exclude contributions from other meteorological processes, particularly winds, regional transport, atmospheric chemistry, and removal.

The corresponding analysis over China also shows substantial interannual variability in SO_2 and the meteorological variables (Fig. 6b). SO_2 column abundance varies across the available TROPOMI record, while temperature, precipitation, and PBLH exhibit their own temporal variability. As over India, no simple one-to-one correspondence is evident between the recent SO_2 behavior and any individual meteorological variable. Figure 6 therefore provides meteorological context for interpreting the

satellite signal, while recognizing that a complete separation of emission-driven and meteorologically driven changes would require a more comprehensive meteorological and chemical-transport attribution analysis.

The March 2025–March 2026 difference maps in Fig. 5 are therefore interpreted as a spatial observational comparison rather than as a statistically attributed conflict signal. Figure 5 characterizes the geographical distribution of the observed SO_2 differences, whereas the longer TROPOMI record in Fig. 6 provides complementary temporal context for the 2026 observations. The accompanying temperature, precipitation, and PBLH anomalies provide additional information on meteorological variability. Together, these spatial and temporal analyses provide complementary constraints on the observed SO_2 changes without assuming that the March 2025–March 2026 difference can be attributed uniquely to geopolitical energy disruption. When considered together with the strong dependence of both countries on Middle Eastern oil imports (Fig. 1) and the substantial contribution of the power sector to regional aerosol loading established independently by the 2023 GEOS-Chem simulations (Fig. 4), the TROPOMI observations are consistent with, but do not by themselves prove, the proposed energy–air-pollution pathway.

An important limitation of the proposed pathway is that the present analysis does not directly demonstrate an increase in coal consumption or coal-fired electricity generation between March 2025 and March 2026, nor does it quantify the magnitude of an actual oil or gas supply disruption during this period. This constitutes the weakest observational link between the geopolitical event and the atmospheric SO_2 signal, and the TROPOMI enhancement should therefore not be interpreted as a proxy for increased coal-fired generation. The strength of the power-sector interpretation also differs substantially between the two countries. In the 2023 CEDS inventory, energy-sector SO_2 emissions account for ~ 5.87 of 9.15 Mt yr^{-1} ($\sim 64\%$) of total SO_2 emissions in India, compared with ~ 2.17 of 10.61 Mt yr^{-1} ($\sim 20\%$) in China (Fig.2). The power-sector interpretation is therefore better supported for India, whereas industrial and other anthropogenic sources constitute a much larger fraction of the SO_2 burden in China. Accordingly, the TROPOMI enhancement over China is interpreted as an atmospheric SO_2 signal potentially influenced by multiple anthropogenic sources rather than specifically as evidence of increased coal-fired power generation. Establishing the missing intermediate link would require contemporaneous information on fuel supply, electricity generation by source, plant utilization, and sector-specific emissions during the conflict period.

The potential air-quality implications of enhanced atmospheric SO_2 are important because SO_2 is a major precursor of sulfate aerosol. If the observed SO_2 enhancement is partly associated with increased sulfur emissions, additional atmospheric oxidation of SO_2 could contribute to sulfate aerosol and secondary $PM_{2.5}$ formation [14,36]. This pathway is particularly relevant for India and China because sulfate constitutes a substantial fraction of their aerosol burden (Figs. 2 and 3), while the GEOS-Chem source-attribution analysis demonstrates an important contribution of power-sector emissions to AOD over major energy-producing regions (Fig. 4). Potential increases in secondary particulate pollution would be of particular concern over densely populated and already polluted regions such as the Indo-Gangetic Plain and North China Plain [10,12]. However, the present study does not directly quantify the resulting changes in $PM_{2.5}$ concentrations or associated population exposure and health burden; these should therefore be regarded as potential implications rather than directly demonstrated outcomes of the present analysis.

Several uncertainties prevent the observed SO_2 enhancement from being interpreted as definitive causal evidence of a Middle East conflict effect. First, TROPOMI measures atmospheric SO_2 column density rather than emission fluxes and does not directly distinguish emissions from power generation, industry, or other sources. Alternative emission-related explanations must also be considered. Changes in industrial activity, domestic energy and emission-control policies, and seasonal biomass-burning emissions during March could contribute to interannual differences in atmospheric SO_2 and associated aerosol loading. These influences may occur independently of, or simultaneously with, changes in power-sector activity and therefore further limit attribution of the observed satellite signal to conflict-related coal utilization. Consequently, the enhancements in Fig. 5 cannot be uniquely attributed to increased coal combustion without contemporaneous sector-resolved emission inventories or dedicated chemical-transport source-attribution simulations. As discussed above, the CEDS sectoral inventory used for our GEOS-Chem analysis currently extends only through 2023, preventing a consistently constrained power-sector simulation for the 2025–2026 period. Applying an assumed post-2023 scaling factor would prescribe rather than independently determine the magnitude of the power-sector emission change.

Second, atmospheric SO_2 columns are influenced by meteorology, transport, chemistry, and removal. Figure 6 explicitly examines temperature and precipitation anomaly as two meteorological factors that could contribute to interannual variability. Although neither variable shows a simple temporal correspondence capable of explaining the observed SO_2 changes by itself, this analysis does not account for all relevant meteorological processes. Variations in boundary-layer height, wind speed and direction, regional transport, humidity, clouds, and oxidation chemistry could alter SO_2 lifetime and spatial distribution. A complete separation of emission-driven and meteorologically driven changes would therefore require additional sensitivity simulations or meteorologically normalized analyses.

Third, the magnitude of any energy-system response to Middle East geopolitical disruption depends on the severity and duration of supply constraints, changes in international energy prices, strategic petroleum and gas reserves, fuel switching, domestic production, electricity demand, and government policy responses. Increased coal utilization would also affect pollutants other than SO_2, including nitrogen oxides, primary particulate matter, and carbonaceous aerosols. Furthermore, differences in emission-control technologies, particularly flue-gas desulfurization and other controls installed at coal-fired power plants, mean that changes in coal consumption do not necessarily translate proportionally into atmospheric SO_2 emissions.

Taken together, our analysis therefore does not interpret the 2025–2026 TROPOMI enhancement as conclusive proof that the ongoing Middle East conflict has caused increased air pollution in India and China. Rather, the results identify an observational signal that is spatially and temporally consistent with a physically plausible energy–air-pollution pathway. The energy-import analysis establishes the vulnerability of India and China to Middle Eastern oil and gas disruptions (Fig. 1), the emission and aerosol analyses demonstrate the importance of fossil-fuel-based power generation for regional sulfur emissions and aerosol loading (Figs. 2–4), TROPOMI identifies enhanced SO_2 during the conflict period over several coal-intensive regions (Fig. 5), and the long-term comparison with temperature and precipitation provides additional meteorological context for interpreting these changes (Fig. 6). Together, these complementary lines of evidence provide a testable framework for assessing how geopolitical energy disruptions may propagate into regional air-quality changes, while emphasizing the need for updated sector-resolved emission inventories and dedicated atmospheric modeling to establish quantitative causal attribution.

Discussion

This study identifies a plausible pathway through which geopolitical disruptions in the Middle East could influence air pollution in India and China by altering energy-use patterns. Rapid economic growth has substantially increased energy demand in both countries, while their energy systems remain dominated by fossil fuels, particularly coal (Fig. 1). At the same time, both countries depend strongly on imported crude oil and natural gas, with the Middle East supplying approximately 45% of India's and 54% of China's crude-oil imports. This combination of external oil and gas dependence and extensive domestic coal infrastructure creates a structural vulnerability whereby prolonged supply disruptions or price shocks could increase reliance on coal-based energy production.

The atmospheric importance of this vulnerability is supported by complementary emission, reanalysis, and modeling evidence. CEDS shows that the power sector is an important source of SO_2, with enhanced emissions concentrated around major coal-fired power-generation regions

(Fig. 2). MERRA-2 further indicates substantial aerosol loading over many of these regions, with sulfate contributing approximately 48% of AOD over India and 42% over China (Fig. 3). The 2023 GEOS-Chem simulations provide more direct source attribution, demonstrating substantial power-sector contributions to AOD over coal-intensive regions of both countries (Fig. 4). The strong spatial agreement between GEOS-Chem and MERRA-2 (R^2 = 0.93 for India and R^2 = 0.92 for China) further supports the model representation of the regional aerosol distribution. Together, these results establish that changes in power-sector emissions have the potential to substantially influence regional aerosol loading.

For the ongoing Middle East conflict period, we deliberately avoid extrapolating the 2023 GEOS-Chem simulations using an assumed emission scaling factor because sector-resolved CEDS emissions are not available beyond 2023. Such an experiment would require prescribing the post-2023 power-sector emission change a priori, while the resulting aerosol response would additionally depend on atmospheric chemistry, transport, meteorology, and removal processes [30,31]. Instead, TROPOMI provides an observational constraint on atmospheric SO_2 during the period of interest. The comparison between March 2025 and March 2026 reveals enhanced SO_2 columns over several coal-intensive regions of India and China, with localized differences reaching approximately 0.6–0.8 DU (Fig. 5). These spatial patterns are consistent with the proposed pathway linking energy-supply disruption, increased importance of coal-based energy, and enhanced sulfur pollution.

Nevertheless, the observed SO_2 enhancement should not be interpreted as direct causal evidence that the Middle East conflict increased coal combustion. The absence of contemporaneous evidence demonstrating both an actual energy-supply disruption and a corresponding increase in coal-fired generation represents the weakest link in the proposed pathway and prevents the atmospheric SO_2 signal from being interpreted as evidence of conflict-induced coal substitution. TROPOMI measures atmospheric SO_2 columns rather than sector-specific emission fluxes, and atmospheric SO_2 is also influenced by meteorology, transport, chemistry, and removal. The long-term comparison with temperature anomaly and precipitation (Fig. 6) does not reveal a simple correspondence between the recent SO_2 changes and either meteorological variable, suggesting that temperature and precipitation alone are unlikely to explain the observed enhancement. However, other meteorological factors, including boundary-layer dynamics, winds, humidity, and regional transport, remain relevant. Updated sector-resolved emission inventories and dedicated chemical-transport sensitivity simulations will therefore be required to establish quantitative causal attribution. The magnitude of any conflict-related energy response also depends on factors beyond the atmospheric system. The severity and duration of supply disruptions, international oil and gas prices, strategic petroleum reserves, alternative suppliers, domestic production, electricity demand, renewable-energy availability, and government intervention can all buffer or amplify changes in fossil-fuel consumption. Moreover, oil, natural gas, and coal are not perfectly interchangeable energy carriers across all sectors. Consequently, the pathway proposed here should not be interpreted as a deterministic sequence in which reduced Middle Eastern oil and gas supply necessarily produces an equivalent increase in coal consumption.

Further, a direct comparison with previous geopolitical conflicts and global oil-market shocks is complicated by substantial differences in the economic scale, energy demand, fuel mix, import structure, emission controls, and observational coverage of India and China across these periods. As shown by the long-term evolution in Fig. 1, both countries currently operate substantially larger energy systems than during earlier conflicts. Moreover, a consistent historical attribution would require event-specific information on oil and gas supply disruptions, import changes, domestic fuel substitution, sectoral emissions, meteorology, and atmospheric composition, which is not consistently available across the historical periods considered here. Previous conflicts should therefore not be treated as direct analogues of the present situation without a dedicated historical attribution framework. A systematic evaluation of such historical energy-supply shocks represents an important direction for future research.

If the observed SO_2 enhancements are partly associated with increased fossil-fuel combustion, their air-quality implications could be important because SO_2 is a major precursor of sulfate and secondary $PM_{2.5}$ [14,36]. This is particularly relevant for already polluted and densely populated regions such as the Indo-Gangetic Plain and North China Plain, where additional sulfur emissions could offset improvements achieved through emission-control policies. The magnitude of such an effect will also depend strongly on plant-level emission controls, particularly flue-gas desulfurization, and therefore changes in coal consumption should not be assumed to translate proportionally into atmospheric SO_2.

The extensive coal-fired power infrastructure in India and China also creates a degree of energy-system lock-in, as substantial generating capacity and associated investments are already established. During periods of external energy-supply uncertainty, this infrastructure can provide short-term flexibility through increased utilization of existing capacity, but prolonged reliance may reinforce high-emission and carbon-intensive energy pathways. Such a response could create challenges for both regional air-quality improvement and longer-term climate-mitigation objectives. The resulting air-quality impact, however, depends strongly on plant-level emission controls, particularly flue-gas desulfurization and other pollution-control technologies. Expanding renewable energy, energy storage, and grid flexibility can therefore reduce the potential trade-off between short-term energy security and longer-term environmental sustainability.

Overall, our results do not establish that the ongoing Middle East conflict has directly caused increased air pollution in India or China. Rather, the combined evidence from energy dependence (Fig. 1), sectoral emissions and aerosol loading (Figs. 2–3), GEOS-Chem power-sector attribution (Fig. 4), TROPOMI SO_2 observations (Fig. 5), and meteorological context (Fig. 6) supports a physically plausible and testable pathway through which geopolitical energy disruptions could affect regional air quality. This integrated framework highlights the broader interconnectedness of geopolitical stability, energy security, and environmental quality, demonstrating why external energy-supply risks should be considered when assessing regional air-quality vulnerability. Developing energy systems that are resilient to external supply shocks while maintaining low emissions can reduce the potential trade-off between energy security and environmental protection. In this context, diversification toward renewable energy, energy storage, grid flexibility, and other low-emission resources can simultaneously strengthen energy-system resilience and support long-term air-quality and climate objectives.

Methods

The analysis integrates complementary international datasets representing different components of the energy–air-pollution system. Our World in Data (OWID) (https://ourworldindata.org/grapher/gdp-per-capita-worldbank-constant-usd) provides long-term economic, electricity, and energy-consumption records; U.S. Energy Information Administration (EIA) country reports characterize fossil-fuel import structures; and the Community Emissions Data System (CEDS)[32] provides sector-resolved anthropogenic emissions. These datasets are further combined with MERRA-2 aerosol reanalysis, GEOS-Chem simulations, and TROPOMI satellite observations to connect energy demand and import dependence with emission sources and atmospheric composition. The individual datasets differ in temporal coverage, spatial resolution, and associated uncertainties, which are described in the corresponding methodological subsections below.

Economic activity: GDP per capita

Economic activity for India and China is represented using gross domestic product (GDP) per capita obtained from the World Bank and compiled by Our World in Data (OWID)[37]. The dataset reports GDP per capita in constant 2015 US dollars, allowing for consistent comparison over time by removing the effects of inflation. Annual data spanning from 1960 to 2023 were used to capture long-term economic growth trends in both countries.

GDP per capita is widely used as an indicator of economic development, reflecting changes in income levels, industrialization, and living

standards. In this study, GDP per capita is used to examine the relationship between economic growth and energy demand, particularly electricity consumption. The data were accessed from the OWID database (https://ourworldindata.org/grapher/gdp-per-capita-worldbank-constant-usd) and processed to extract country-specific time series for India and China.

To ensure consistency with the energy datasets, GDP values were temporally aligned and analyzed alongside electricity demand and total energy consumption. GDP per capita in constant 2015 US dollars provides a long-term indicator of economic development while accounting for the effects of inflation, thereby enabling consistent temporal comparison. The co-evolution of GDP per capita and energy demand is used to provide economic context for the substantial expansion of the energy systems of India and China. No additional normalization was applied because the GDP dataset is already reported in constant-dollar units.

Electricity demand, generation, production

Electricity demand, generation, and production data for India and China were obtained from the Our World in Data (OWID) database, which compiles information from international energy statistics, including the International Energy Agency (IEA) and other national sources. Electricity demand data were retrieved from the OWID dataset (https://ourworldindata.org/grapher/electricity-demand), while electricity production by source (including coal, oil, gas, hydropower, nuclear, wind, and solar) was obtained from (https://ourworldindata.org/grapher/electricity-production-by-source).

The datasets provide annual electricity demand (TWh)[38] and production disaggregated by energy source over the period 1965-2023, enabling long-term analysis of energy system evolution. Electricity demand represents total consumption, whereas electricity production is categorized by fuel type, allowing assessment of the relative contribution of fossil fuels and non-fossil sources.

For this study, country-specific time series for India and China were extracted and analyzed to examine the relationship between economic growth and electricity demand, as well as the evolution of energy sources used for power generation. Particular emphasis was placed on coal-based electricity production, given its dominant role in both countries. The data were temporally aligned with GDP and emission datasets to ensure consistency across analyses. No additional normalization was applied, as the datasets are reported in standardized physical units (TWh).

Energy consumption by sources

Energy consumption by source for India and China was obtained from the Our World in Data (OWID) database, which compiles data from the Energy Institute's Statistical Review of World Energy and other international energy statistics[39]. The dataset (https://ourworldindata.org/grapher/energy-consumption-by-source-and-country) provides annual primary energy consumption disaggregated by source, including coal, oil, natural gas, hydropower, nuclear, wind, and solar.

The data are reported in terawatt-hours (TWh)[39] and span the period 1965-2023, enabling long-term assessment of changes in the energy mix. For this study, country-specific time series were extracted to quantify the relative contributions of different energy sources and to evaluate the dominance of fossil fuels, particularly coal, in meeting growing energy demand.

The dataset was used to construct the temporal evolution of energy consumption (Fig. 1c,d) and to calculate the fractional contribution of each energy source to total consumption. These data were further integrated with electricity generation, GDP, and emission datasets to examine the linkages between economic growth, energy use, and air pollution. No additional normalization was applied, as the data are reported in consistent physical units.

Energy imports from the Middle East and other countries by India and China

Data on fossil fuel imports for India and China were obtained from country-level energy reports published by the U.S. Energy Information Administration (EIA). Specifically, import shares of crude oil, natural gas, and coal by source country were extracted from graphical representations provided in the EIA country analysis reports for India (https://www.eia.gov/international/content/analysis/countries_long/India/pdf/India.pdf) and China (https://www.eia.gov/international/content/analysis/countries_long/China/pdf/China-2025.pdf). Since the underlying numerical data for some of the import-source distributions were not directly available in tabulated form, the corresponding shares of crude oil, natural gas, and coal imports were digitized from graphical information presented in the EIA country reports. This procedure introduces uncertainty associated with graphical resolution, identification of category boundaries, rounding in the original figures, and the digitization process. The extracted percentages should therefore be interpreted as approximate estimates rather than exact import shares. These data are used primarily to characterize the broad geographical structure of fossil-fuel imports and the relative importance of Middle Eastern suppliers, rather than for high-precision calculations of energy flows or quantitative attribution of atmospheric changes. Particular emphasis was placed on quantifying the dependence on Middle Eastern energy supplies, given their relevance to potential geopolitical disruptions. While minor uncertainties may arise from the digitization of graphical data, the extracted values provide a useful representation of the overall import structure and regional dependencies. These data were integrated with energy consumption and emission datasets to assess the vulnerability of India and China to external energy supply shocks and their potential implications for shifts in domestic fuel use and air pollution.

Spatial distribution of gas, oil, coal-fired power plants

The spatial distribution of gas-, oil-, and coal-fired power plants was obtained from the Global Power Plant Database developed by the World Resources Institute (WRI) (https://datasets.wri.org/datasets/global-power-plant-database). This dataset provides georeferenced information on power plants worldwide, including plant location (latitude and longitude), primary fuel type, and installed capacity.

For this study, power plant data for India and China were extracted and filtered based on fuel type to include coal, oil, and natural gas-fired facilities. The dataset was used to map the spatial distribution of thermal power plants and to assess their clustering across major industrial and energy-producing regions. Installed capacity (MW) was also used to classify plant sizes and to highlight regions with high-density, large-capacity power generation infrastructure.

The processed data were used to generate spatial maps of thermal power plants (Fig. 1e,f), illustrating the concentration of coal-based power generation in key regions of India and China. These spatial distributions were further analyzed in conjunction with SO_2 emissions and aerosol loading to establish the linkage between energy infrastructure and air pollution patterns.

While the dataset provides comprehensive global coverage, minor uncertainties may arise due to differences in reporting years and completeness across regions. Nevertheless, it represents one of the most consistent and widely used sources for assessing the global distribution of power generation infrastructure.

Community emissions data system (CEDS) emissions of SO_2 from different sectors

Sectoral emissions of sulfur dioxide (SO_2) were obtained from the Community Emissions Data System (CEDS)[32], which provides global, gridded emission inventories with sectoral disaggregation. The CEDS dataset includes anthropogenic emissions from multiple sectors, including energy production, industry, residential, transportation, and other sources, with annual temporal resolution.

For this study, SO_2 emissions for India and China were extracted over the period 1900–2023 to capture long-term trends associated with industrialization and energy use. Emissions are reported in mass units (typically tonnes yr^{-1}) and are spatially resolved on a global grid, enabling both temporal and spatial analysis. Sectoral contributions were analyzed to quantify the relative importance of energy-related emissions, particularly from fossil fuel combustion, in driving total SO_2 emissions.

The dataset was used to construct time series of sectoral SO_2 emissions (Fig. 2a,b) and to generate spatial emission maps (Fig. 2c,d), highlighting regional hotspots and their association with major energy-producing regions. Particular emphasis was placed on emissions from the energy sector, given its dominant role in coal-based power generation.

The CEDS inventory integrates information from energy statistics, emission factors, and activity data, ensuring consistency across countries and time. While uncertainties may arise from emission factor assumptions and sectoral allocation, CEDS provides one of the most comprehensive and widely used datasets for analyzing long-term trends in anthropogenic emissions. These data were further integrated with satellite observations and energy datasets to examine the linkage between fossil fuel use and air pollution.

Aerosol optical depth and its composition from MERRA-2 and CMIP6

Aerosol optical depth (AOD) and its compositional components were obtained from the Modern-Era Retrospective analysis for Research and Applications, Version 2 (MERRA-2) [40,41] and simulations from the Coupled Model Intercomparison Project Phase 6 (CMIP6) [42]. MERRA-2 assimilates aerosol-related satellite observations within the GEOS atmospheric modeling and data-assimilation system. Total AOD is therefore observationally constrained through the assimilation framework, whereas the individual aerosol components, including sulfate, black carbon, organic carbon, dust, and sea salt, are model-derived speciated fields and should not be interpreted as direct observations of aerosol composition.

CMIP6 simulations were used to characterize the longer-term evolution of AOD and its components. Historical simulations were used through the end of the CMIP6 historical period, after which output from the SSP2-4.5 ScenarioMIP experiment was used to extend the time series [43]. SSP2-4.5 represents a medium-forcing CMIP6 pathway and provides a continuation of the historical simulations beyond 2014/2015. The resulting long-term record therefore combines historical model output with scenario-based projections for the subsequent period and should not be interpreted as an entirely observational or historical AOD record.

Multi-year averages (2000–2024) were calculated to characterize the mean spatial distribution of AOD and its components (Fig. 3) from MERRA2, while linear trends over the same period were derived to assess temporal changes (Fig. 3). Time series analysis was also performed to examine the evolution of total AOD and its composition (Fig. 2e,f). The relative contribution of each component to total AOD was computed to identify dominant aerosol types in different regions.

MERRA-2 assimilates satellite observations[41] and ground-based AErosol RObotic NETwork (AERONET) measurements[44], including aerosol optical properties, providing a robust representation of atmospheric aerosols[41]. However, uncertainties may arise from model parameterizations, emission inputs, and representation of aerosol processes[41,45]. CMIP6[42] simulations also introduce uncertainties related to model structure and forcing scenarios. Despite these limitations, the combined use of reanalysis and model data provides a comprehensive framework for assessing aerosol trends and their linkage to emissions and energy use.

The statistical significance of trends in aerosol optical depth and its components was calculated by using a linear regression approach[46,47]. For each grid cell, a least-squares linear fit was applied to the time series (2000–2024) to estimate the trend (slope), and the significance of the trend was assessed using a two-tailed Student's t-test[46,48]. Trends with p-values less than 0.05 ($p \le 0.05$) were considered statistically significant[46,48]. The resulting significance was spatially mapped, with statistically significant regions indicated by black dots in Figs. S1 and S2. This approach allows identification of regions where observed changes in AOD and its components are robust and unlikely to arise from natural variability.

GEOS-Chem modeling and source-specific aerosol contribution

The contribution of power-sector emissions to regional aerosol loading was investigated using the GEOS-Chem chemical transport model (v12.2.1) [31]. The model was configured with aerosol chemistry to represent the transport, chemical transformation, and removal of major aerosol species. Meteorological fields were supplied by the MERRA-2 reanalysis. Regional nested simulations were performed at a horizontal resolution of 0. 5° × 0.625° with 47 vertical levels extending from the surface to approximately 0.01 hPa. Meteorological and chemical boundary conditions for the nested domains were obtained from a global GEOS-Chem simulation conducted at 2° × 2. 5° resolution.

The source-attribution experiment was conducted for 2023, corresponding to the most recent year for which the sector-resolved CEDS emissions used in this analysis were available. A reference simulation containing the complete emission inventory was compared with a perturbation simulation in which power-sector emissions were removed. Power-sector-attributable AOD was calculated as the difference between the reference and power-sector-zero-out simulations, and its percentage contribution was calculated relative to total AOD in the reference simulation. This approach provides a model-based estimate of the sensitivity of regional aerosol loading to power-sector emissions.

Anthropogenic emissions were prescribed using the Community Emissions Data System version 2 (CEDSv2) inventory[49]. The model additionally represents natural and biogenic emission sources, including mineral dust, biogenic volatile organic compounds, sea salt, soil NO_x, volcanic emissions, and biomass burning. Biogenic emissions were represented following[50], while biomass-burning emissions were obtained from the Global Fire Emissions Database version 4 (GFEDv4)[51].

The power-sector percentages derived from the zero-out experiments should be interpreted as model-based source-attribution estimates rather than exact observational fractions. Comparison with MERRA-2 indicates that GEOS-Chem reproduces the dominant spatial variability in AOD ($R^2 = 0.93$ over India and $R^2 = 0.92$ over China), but regression slopes of 1.22 and 1.32, respectively, indicate a positive model bias across the comparison range. This bias introduces uncertainty into the absolute magnitude of simulated AOD and consequently into the quantitative power-sector contribution. In addition, the zero-out approach diagnoses the atmospheric response to removing power-sector emissions within the modeled chemical environment. Because secondary aerosol formation can respond nonlinearly to changes in precursor emissions, individual sectoral contributions are not necessarily strictly additive. The percentage-contribution maps in Fig. 4 are therefore used to identify the spatial importance and approximate magnitude of the modeled power-sector influence rather than as exact observational source fractions.

Tropospheric monitoring instrument (TROPOMI) instrument observed SO_2

Tropospheric sulfur dioxide (SO_2) column densities were obtained from the Tropospheric Monitoring Instrument (TROPOMI)[52] onboard the Sentinel-5 Precursor satellite. TROPOMI provides daily global coverage with high spatial resolution (up to ~ 3.5 × 5.5 km^2 at nadir), enabling detailed monitoring of atmospheric trace gases, including SO_2, from both anthropogenic and natural sources.

SO_2 vertical column densities were retrieved using ultraviolet (UV) spectral measurements based on differential optical absorption spectroscopy (DOAS)[53]. The data used in this study correspond to the Level-2 SO_2 products, which include slant column densities converted to vertical column densities using air mass factors that account for viewing geometry, surface reflectivity, and atmospheric conditions.

To ensure data quality and consistency, TROPOMI observations were processed using the HARP (Harmonized Atmospheric Retrievals for Pollution) toolkit (https://atmospherictoolbox.org/media/usecases/Usecase_1_S5P_SO2_La_Soufriere.html). HARP provides standardized tools for filtering, regridding, and harmonizing satellite data. Quality assurance filtering was applied using the SO_2 quality flag (qa_value), and only pixels with qa_value > 0.5 were retained. The TROPOMI SO_2 observations used in this study were obtained from the Sentinel-5P reprocessed (RPRO) Level-2 SO_2 product. The product files used in the analysis correspond to processor/

product version 02.08.00. Following quality filtering, the observations were regridded onto a regular latitude–longitude grid to facilitate the calculation of monthly means and comparison with model and emission datasets. The data were subsequently regridded onto a regular latitude–longitude grid to facilitate spatial averaging and comparison with model and emission datasets. Mean SO_2 column densities were calculated over India and China using quality-filtered TROPOMI observations for the period 1–20 March in both 2025 and 2026. Using the same calendar-day window in both years ensures a temporally consistent comparison and minimizes differences associated with unequal sampling periods and the seasonal cycle. The 1–20 March 2025 period is used as the pre-conflict/reference period, whereas 1–20 March 2026 represents the conflict-period observation considered in this study. Spatial distributions and 2026 minus 2025 difference maps were generated for these matched 20-day periods to characterize regional changes in atmospheric SO_2 column abundance (Fig. 5). These observations provide direct constraints on atmospheric SO_2 variability; however, they represent atmospheric column abundance rather than sector-specific emission fluxes and therefore cannot independently identify the emission source responsible for an observed enhancement. While TROPOMI provides high-resolution and near-real-time observations, uncertainties remain due to retrieval assumptions, cloud interference, air-mass-factor assumptions, and sensitivity to boundary-layer SO_2. These retrieval-related uncertainties should therefore be considered when interpreting spatial and temporal variations in the satellite-derived SO_2 columns.

Meteorological data: temperature, precipitation, and planetary boundary-layer height

Meteorological variability was characterized using near-surface air temperature and precipitation from the Climatic Research Unit Time-Series (CRU TS) version 4.10 dataset [54], together with planetary boundary-layer height (PBLH) obtained from the ERA5 global atmospheric reanalysis [55]. These meteorological variables were used to provide additional context for interpreting the temporal variability in TROPOMI-observed SO_2 over India and China (Fig. 6), rather than to perform a complete meteorological normalization of the satellite observations.

CRU TS v4.10 provides monthly gridded climate fields at a horizontal resolution of 0. 5° × 0. 5°. Near-surface air temperature and precipitation were extracted over India and China, and country-level spatial averages were calculated for each time step. The temperature variable represents near-surface air temperature and is reported in degrees Celsius, while precipitation is reported in millimetres. The CRU TS data were analyzed over the period 2000–2026 to characterize longer-term variability in temperature and precipitation over the two countries.

Planetary boundary-layer height was obtained from ERA5[55] and analyzed over the same 2000–2026 period. PBLH provides additional information on variations in the vertical mixing depth of the lower atmosphere and is therefore relevant when interpreting changes in near-surface pollutant accumulation and atmospheric column abundance. ERA5 PBLH fields were spatially averaged separately over India and China to generate country-level time series consistent with the temperature and precipitation analyses.

Temperature, precipitation, and PBLH anomalies were calculated relative to their respective mean conditions over the full 2000–2026 analysis period. This reference period was selected to characterize departures from the longer-term meteorological state and should not be interpreted as a pre-conflict baseline. Although 2026 is included in the reference period, it represents only one year of the 27-year analysis-period mean and therefore has a limited influence on the reference value. The longer meteorological records provide context for interannual variability, whereas the TROPOMI SO_2 observations used in this study span 2019–2026.

The resulting temperature, precipitation, and PBLH anomalies were analyzed together with the TROPOMI SO_2 time series to examine whether the recent SO_2 changes coincided with pronounced variations in these meteorological conditions (Fig. 6). These variables represent important, but not exhaustive, controls on atmospheric SO_2. Other processes, including wind speed and direction, regional transport, humidity, cloud processes, atmospheric chemistry, and wet and dry removal, may also influence SO_2 abundance. Consequently, the meteorological analysis is used to provide context for the observed SO_2 variability and is not used to establish or exclude causal attribution to the ongoing geopolitical conflict.

Data availability

All data used in this study are publicly available from the following sources. GDP per capita data were obtained from the World Bank and compiled by Our World in Data (OWID) (https://ourworldindata.org/grapher/gdp-per-capita-worldbank-constant-usd). Electricity demand and generation data were retrieved from OWID (https://ourworldindata.org/grapher/electricity-demand; https://ourworldindata.org/grapher/electricity-production-by-source). Energy consumption by source was obtained from OWID (https://ourworldindata.org/grapher/energy-consumption-by-source-and-country). Data on fossil fuel imports for India and China were extracted from graphical information provided in U.S. Energy Information Administration (EIA) country reports (https://www.eia.gov/international/content/analysis/countries_long/India/pdf/India.pdf; https://www.eia.gov/international/content/analysis/countries_long/China/pdf/China-2025.pdf). Spatial data on power plants were obtained from the Global Power Plant Database by the World Resources Institute (WRI) (https://datasets.wri.org/datasets/global-power-plant-database). Sectoral SO2 emissions were obtained from the Community Emissions Data System (CEDS) at https://www.ccacoalition.org/resources/community-emissions-data-system-ceds-historical-emissions. Aerosol optical depth (AOD) and its components from CMIP6 are obtained from https://esgf-data.dkrz.de/projects/cmip6-dkrz/CMIP6 ESGF archive, and MERRA-2 aerosol reanalysis data are obtained from https://goldsmr4.gesdisc.eosdis.nasa.gov/data/MERRA2_MONTHLY/M2TMNXAER.5.12.4/ NASA MERRA-2 archive. Satellite observations of SO2were obtained from the Tropospheric Monitoring Instrument (TROPOMI) onboard Sentinel-5P, available at https://www.earthdata.nasa.gov/data/instruments/tropomi/near-real-time-data. The CRU temperature and precipitation are obtained from https://badc.nerc.ac.uk/data/cru/. The PBLH data has been obtained from ERA5 available at https://cds.climate.copernicus.eu/datasets/reanalysis-era5-single-levels?tab=download.

Code availability

All the plots are generated using Python version 3.5.

Received: 31 March 2026; Accepted: 8 October 2026;
Published online: 05 November 2026

References

1. Liu, H., Lei, M., Zhang, N. & Du, G. The causal nexus between energy consumption, carbon emissions and economic growth: New evidence from China, India and G7 countries using convergent cross mapping. *PLoS One* **14**, e0217319 (2019).
2. Jóźwik, B., Panda, S. P., Dash, A. K., Sahu, P. K. & Szwed, R. Revisiting the nexus between energy consumption, economic growth, and co2 emissions in India and China: Insights from the long short-term memory (LSTM) model. *Energies* **18**, 4167 (2025).
3. Ahmed, M., Shuai, C. & Ahmed, M. Influencing factors of carbon emissions and their trends in China and India: a machine learning method. *Environ. Sci. Pollut. Res.* **29**, 48424–48437 (2022).
4. Li, C. et al. Reversal of trends in global fine particulate matter air pollution. *Nat. Commun.* **14**, 5349 (2023).
5. Swain, B. et al. Economic-boom-driven electricity demand linked to urban air pollution and health in India. Nature Cities1-16 (2026).
6. Jones, D. W. How urbanization affects energy-use in developing countries. *Energy Policy* **19**, 621–630 (1991).
7. Poumanyvong, P. & Kaneko, S. Does urbanization lead to less energy use and lower co2 emissions? A cross-country analysis. *Ecol. Econ.* **70**, 434–444 (2010).

8. Tong, D. et al. Committed emissions from existing energy infrastructure jeopardize 1.5 c climate target. *Nature* **572**, 373–377 (2019).
9. Xie, Y. et al. Large-scale renewable energy brings regionally disproportional air quality and health co-benefits in China. *iScience* **26**, 107459 (2023).
10. Anchan, N. L. et al. Assessing the variability of aerosol optical depth over India in response to future scenarios: Implications for carbonaceous aerosols. *J. Geophys. Res. Atmos.* **129**, e2024JD040846 (2024).
11. Singh, A. et al. Rapid growth and high cloud-forming potential of anthropogenic sulfate aerosol in a thermal power plant plume during COVID lockdown in India. *npj Clim. Atmos. Sci.* **6**, 109 (2023).
12. Malasani, C. R. et al. Modeling of mercury deposition in India: evaluating emission inventories and anthropogenic impacts. *Environ. Sci. Process. Impacts* **26**, 1999–2009 (2024).
13. Lelieveld, J., Evans, J. S., Fnais, M., Giannadaki, D. & Pozzer, A. The contribution of outdoor air pollution sources to premature mortality on a global scale. *Nature* **525**, 367–371 (2015).
14. Zhang, Q. et al. Drivers of improved pm2. 5 air quality in China from 2013 to 2017. *Proc. Natl. Acad. Sci. USA*. **116**, 24463–24469 (2019).
15. Agency, I. E. *World energy outlook* (OECD/IEA Paris, 2009).
16. Vivoda, V. Evaluating energy security in the Asia-Pacific region: a novel methodological approach. *Energy Policy* **38**, 5258–5263 (2010).
17. Gupta, E. Oil vulnerability index of oil-importing countries. *Energy Policy* **36**, 1195–1211 (2008).
18. Song, R. et al. Coal plants persist as a large barrier to the global solar energy transition. *Nat. Sustain.* **9**, 981–992 https://doi.org/10.1038/s41893-026-01836-5 (2026).
19. Luft, G. Dependence on Middle East energy and its impact on global security. In Stec, S. & Baraj, B. (eds.) *Energy and Environmental Challenges to Security*, 197–210 https://doi.org/10.1007/978-1-4020-9453-8_13 (Springer, 2009).
20. Colgan, J. D. Oil, domestic politics, and international conflict. *Annu. Rev. Political Sci.* **17**, 189–209 https://doi.org/10.1146/annurev-polisci-071112-213701 (2014).
21. Hamilton, J. D. Causes and consequences of the oil shock of 2007-08. Tech. Rep., National Bureau of Economic Research (2009).
22. Kilian, L. The economic effects of energy price shocks. *J. Econ. Lit.* **46**, 871–909 (2008).
23. He, K., Huo, H. & Zhang, Q. Urban air pollution in China: current status, characteristics, and progress. *Annu. Rev. Energy Environ.* **27**, 397–431 (2002).
24. Gunthe, S. S. et al. Enhanced aerosol particle growth sustained by high continental chlorine emission in India. *Nat. Geosci.* **14**, 77–84 (2021).
25. Patel, A. et al. Linking anthropogenic chlorine emissions to regional air quality in India. *npj Clean. Air* **2**, 23 https://doi.org/10.1038/s44407-026-00066-5 (2026).
26. Vaishya, A. et al. Black carbon over tropical Indian coast during the COVID-19 lockdown: inconspicuous role of coastal meteorology. *Environ. Sci. Pollut. Res.* **30**, 44773–44781 (2023).
27. Hu, W. et al. Health burdens related to emission sources and cross-provincial air pollution in China. *npj Clim. Atmos. Sci.* **7**, 312 (2024).
28. Chen, Y. et al. Substantial differences in source contributions to carbon emissions and health damage necessitate balanced synergistic control plans in China. *Nat. Commun.* **15**, 5880 (2024).
29. Zheng, Y. et al. Air quality improvements and health benefits from China's clean air action since 2013. *Environ. Res. Lett.* **12**, 114020 (2017).
30. Norman, O. G. et al. Exploring the processes controlling secondary inorganic aerosol: evaluating the global geos-chem simulation using a suite of aircraft campaigns. *Atmos. Chem. Phys.* **25**, 771–795 (2025).
31. Bey, I. et al. Global modeling of tropospheric chemistry with assimilated meteorology: Model description and evaluation. *J. Geophys. Res. Atmos.* **106**, 23073–23095 (2001).
32. McDuffie, E. E. et al. A global anthropogenic emission inventory of atmospheric pollutants from sector-and fuel-specific sources (1970–2017): an application of the Community Emissions Data System (CEDS). *Earth Syst. Sci. Data* **12**, 3413–3442 (2020).
33. Ministry of Power, Government of India. Annual report 2024–25 (2025).
34. International Energy Agency. India energy outlook 2021 (2021).
35. International Energy Agency. Coal 2023: Analysis and forecast to 2026 (2023).
36. Wang, Y. et al. The ion chemistry and the source of pm2. 5 aerosol in Beijing. *Atmos. Environ.* **39**, 3771–3784 (2005).
37. National statistical organizations and central banks, OECD national accounts & World Bank staff estimates. GDP per capita—World Bank—In constant US$. https://archive.ourworldindata.org/20260304-094028/grapher/gdp-per-capita-worldbank-constant-usd.html Dataset, with minor processing by Our World in Data (2026).
38. Ember & Energy Institute. Electricity generation from coal. https://ourworldindata.org/grapher/electricity-production-by-source (2026).
39. Energy Institute. Other renewables (including geothermal and biomass). https://ourworldindata.org/grapher/energy-consumption-by-source-and-country Dataset, with major processing by Our World in Data. Original data from Energy Institute, Statistical Review of World Energy (2025).
40. Gelaro, R. et al. The modern-era retrospective analysis for research and applications, version 2 (MERRA-2). *J. Clim.* **30**, 5419–5454 (2017).
41. Reichle, R. H. et al. Assessment of MERRA-2 land surface hydrology estimates. *J. Clim.* **30**, 2937–2960 (2017).
42. Eyring, V. et al. Overview of the coupled model intercomparison project phase 6 (CMIP6) experimental design and organization. *Geosci. Model Dev.* **9**, 1937–1958 (2016).
43. O'Neill, B. C. et al. The scenario model intercomparison project (scenariomip) for CMIP6. *Geosci. Model Dev.* **9**, 3461–3482 https://doi.org/10.5194/gmd-9-3461-2016 (2016).
44. Holben, B. N. et al. AERONET—a federated instrument network and data archive for aerosol characterization. *Remote Sens. Environ.* **66**, 1–16 (1998).
45. Malasani, C. R. et al. Meteorological evaluation of the MERRA-2 reanalysis dataset: Insights for the Indian subcontinent. *EGUsphere* **2025**, 1–31 (2025).
46. Wilks, D. S.*Statistical methods in the atmospheric sciences*, vol. 100 (Academic Press, 2011).
47. Santer, B. D. et al. Statistical significance of trends and trend differences in layer-average atmospheric temperature time series. *J. Geophys. Res. Atmos.* **105**, 7337–7356 (2000).
48. Student. The probable error of a mean. *Biometrika***6**, 1–25 (1908).
49. Hoesly, R. M. et al. Historical (1750–2014) anthropogenic emissions of reactive gases and aerosols from the community emissions data system (ceds). *Geosci. Model Dev.* **11**, 369–408 (2018).
50. Guenther, A. B. et al. The model of emissions of gases and aerosols from nature version 2.1 (MEGAN2.1): an extended and updated framework for modeling biogenic emissions. *Geosci. Model Dev.* **5**, 1471–1492 (2012).
51. Giglio, L., Randerson, J. T. & Van Der Werf, G. R. Analysis of daily, monthly, and annual burned area using the fourth-generation global fire emissions database (GFED4). *J. Geophys. Res. Biogeosci.* **118**, 317–328 (2013).
52. Veefkind, J. P. et al. Tropomi on the ESA Sentinel-5 precursor: A gmes mission for global observations of the atmospheric composition for climate, air quality and ozone layer applications. *Remote Sens. Environ.* **120**, 70–83 (2012).
53. Platt, U. Differential optical absorption spectroscopy (DOAS). In Sigrist, M. W. (ed.) *Air Monitoring by Spectroscopic Techniques*, 27–84 (John Wiley & Sons, New York, 1994).
54. Harris, I., Osborn, T. J., Jones, P. & Lister, D. Version 4 of the CRU TS monthly high-resolution gridded multivariate climate dataset. *Sci. Data* **7**, 109 https://doi.org/10.1038/s41597-020-0453-3 (2020).

55. Hersbach, H. et al. The ERA5 global reanalysis. *Q. J. R. Meteorol. Soc.* **146**, 1999–2049 https://doi.org/10.1002/qj.3803 (2020).

Acknowledgements
The authors acknowledge the use of publicly available datasets from Our World in Data (OWID), the U.S. Energy Information Administration (EIA), the World Resources Institute (WRI), the Community Emissions Data System (CEDS), MERRA-2 reanalysis, CMIP6 simulations, and the Tropospheric Monitoring Instrument (TROPOMI) onboard Sentinel-5P.

Author contributions
B.S. and M.V. conceived and designed the research undertaken in this study. B.S. and M.V. analyzed the datasets and generated the plots. All the co-authors, D.T., A.S., A.D., M.V., A.P., C.R.M., L.L., A.T., and S.S.G., helped in shaping the manuscript. All authors contributed to the interpretation of the results and the preparation of the final manuscript.

Funding
Open Access funding enabled and organized by Projekt DEAL.

Competing interests
The authors declare no competing interests.

Additional information
Supplementary information The online version contains supplementary material available at https://doi.org/10.1038/s44407-026-00112-2.

Correspondence and requests for materials should be addressed to Basudev Swain, Marco Vountas or Luca Lelli.

Reprints and permissions information is available at http://www.nature.com/reprints

Publisher's note Springer Nature remains neutral with regard to jurisdictional claims in published maps and institutional affiliations.

Open Access This article is licensed under a Creative Commons Attribution 4.0 International License, which permits use, sharing, adaptation, distribution and reproduction in any medium or format, as long as you give appropriate credit to the original author(s) and the source, provide a link to the Creative Commons licence, and indicate if changes were made. The images or other third party material in this article are included in the article's Creative Commons licence, unless indicated otherwise in a credit line to the material. If material is not included in the article's Creative Commons licence and your intended use is not permitted by statutory regulation or exceeds the permitted use, you will need to obtain permission directly from the copyright holder. To view a copy of this licence, visit http://creativecommons.org/licenses/by/4.0/.

© The Author(s) 2026